Original Article

![CAMBRIDGE UNIVERSITY PRESS]

Long duration ~600–500 Ma high-T metamorphism ended with early Ordovician rapid intermediate-T cooling and stabilization of Sri Lanka in central Gondwana

Daniel K. Holm[1] , Inoka Widanagamage[1], Nelia Dunbar[2] and Matthew Heizler[2]

[1]Department of Earth Sciences, Kent State University, Kent, OH, USA and [2]New Mexico Bureau of Geology and Mineral Resources and Department of Earth and Environmental Science, New Mexico Institute of Mining and Technology, Socorro, NM, USA

Abstract

Continent formation and its stabilization are key factors for understanding tectonic processes and histories across geologic time. Sri Lanka consists of a Central Highland (HC) granulite/UHT terrane bounded by tectonic sutures and medium-to-high-grade magmatic arc terranes likely formed via Neoproterozoic double-sided subduction and collision associated with assembly of Gondwana. EMP Chemical Th-U-Pb dating of monazite within the eastern suture is dominated by 595–635 Ma dates, consistent with juxtaposition ca. 600 Ma as arc magmatism ended. Chemical analysis of metamorphic monazite dates from the eastern HC indicates prograde HT metamorphism (M1) at ca. 570 Ma during garnet growth (lower Y monazite) and retrograde HT metamorphism (M2) at ca. 560–550 Ma (higher Y monazite). These ages reflect orogenic thickening associated with arc collisions (M1) and retrograde metamorphism (M2) during deep-crustal exhumation of HC rocks. Regional long duration (>50–100 Ma) HT metamorphism, which continued until 520 Ma, and possibly to ca. 480 Ma, was followed shortly by rapid early Ordovician (480–490 Ma) lower to mid-crustal cooling based on near concordant ^{40}Ar-^{39}Ar hornblende and biotite ages. Rapid cooling occurred concurrently with metasomatism (He *et al.* 2016), and region-wide exhumation during orogenic collapse documented in adjacent portions of Gondwana. The cessation of long-duration HT metamorphism linked to the onset of rapid Ordovician intermediate-temperature (>500–<300 °C) cooling and exhumation via orogenic collapse resulted in young stabilized continental crust. The Neoproterozoic-Early Palaeozoic metamorphic/thermal evolution of Sri Lanka (and correlated regions) within Gondwana attests to the timing and process of rapid stabilization of central Gondwanaland.

1. Introduction

Continent formation and its stabilization are key factors for understanding tectonic processes and histories across geologic time (Nelson, 1991; Holm *et al.* 1998, 2020;). The Neoproterozoic crustal block of Sri Lanka is well suited for investigating how volcanic arcs are transformed tectonically via accretion/collisions, high-T metamorphism, intense deformation and ultimately stabilized into continental crust. Late Neoproterozoic continental reconstructions place the continental fragment of Sri Lanka at the nexus of Africa, Madagascar, India and East Antarctica in the heart of the Gondwana supercontinent (Fig. 1; Yoshida *et al.* 1992; Lawver *et al.* 1998). Geological correlations of Sri Lanka with adjacent Gondwana fragments (the Lützow-Holm Complex (LHC) in East Antarctica (Yoshida *et al.* 1992; Shiraishi *et al.* 1994), the Kerala Khondalite Belt (KKB) in southern India (Plavsa *et al.* 2014; Kitano *et al.* 2018), the Lurio foreland (LF) of Mozambique (Ng *et al.* 2017) and southern Madagascar (MD; Jöns & Schenk, 2011; Fitzsimmons, 2016) are based, in part, on similarities of lithologies, structures, Neoproterozoic arc magmatism and age of UHT metamorphism. The geology and central position of Sri Lanka within Gondwana underscores its importance for documenting and better understanding continental growth (via arc formation and amalgamation) during supercontinent assembly, and its subsequent stabilization.

Representing a collage of subduction-related igneous and highly deformed and metamorphosed sedimentary middle and lower-crustal rocks, our understanding of the tectonometamorphic history of Sri Lankan basement rocks has been significantly advanced by U-Pb zircon geochronologic research over the past two decades. SIMS, SHRIMP and LA-ICPMS zircon U-Pb analyses from basement rocks of central and eastern Sri Lanka (Sajeev *et al.* 2007, 2010; Dharmapriya *et al.* 2015; He *et al.* 2016; Ng *et al.* 2017) indicate a dominant latest Neoproterozoic-Cambrian UHT and granulite metamorphism interpreted to be associated with double-sided arc accretion during closure of the southern Mozambique Ocean (Santosh *et al.* 2014; He *et al.* 2018).
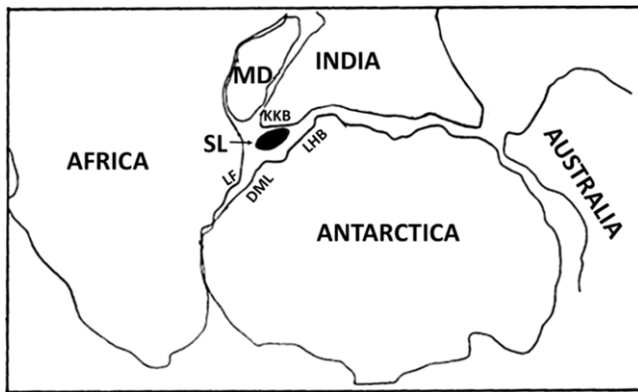
Figure 1. Gondwana reconstruction after Lawver *et al.* (1998). MD = Madagascar; SL = Sri Lanka, DML = Dronning Maud Land; LHB = Lützow-Holm Belt; KKB = Kerala Khondalite Belt.

In comparison, few conventional U-Pb monazite dates have been reported from Sri Lankan basement rocks. Hölzl *et al.* (1994) obtained monazite TIMS ages of 592 and 555 Ma from metapelitic granulites of the central Highland Complex (HC). Sajeev *et al.* (2010) obtained uniform SHRIMP U-Pb monazite ages of ca. 550 Ma on retrograde monazite grains, concordant with SHRIMP U-Pb zircon overgrowth ages in UHT rocks in central Sri Lanka (HC). CHIME monazite dating (Malaviarachchi & Takasu, 2011) yielded a wider range of metamorphic ages between 730 and 460 Ma, although HC detrital zircon ages as young as 800–600 Ma (Takamura *et al.* 2016) suggest the older (730–600 Ma) components may be relic detrital monazite. Despite its potential as a rapid and non-destructive high-resolution geochronometer, particularly in Proterozoic crustal studies, no electron microprobe (EMP) monazite ages have been obtained from Sri Lankan basement rocks. Here we report EMP monazite ages from southeast Sri Lanka and compare these ages with prior M1 (prograde) and M2 (retrograde) zircon metamorphic ages from central Sri Lanka.

Little is known about the post UHT metamorphic exhumation and stabilization of the Sri Lankan complexes despite its importance in documenting and understanding the post-collisional/orogenic history following Gondwana assembly, stabilization and break-up. The post-peak metamorphic (<550 Ma) mid-crustal cooling history in Sri Lanka is currently poorly constrained by a few early K-Ar and Rb-Sr mineral (dominantly biotite) ages and unpublished ^{40}Ar-^{39}Ar laser microprobe mineral ages which collectively scatter between ca. 550–420 Ma (Cooray, 1969; Hölzl *et al.* 1991; Burton & O'Nions, 1990; Irwin *et al.* 1987). Here we report the first ^{40}Ar-^{39}Ar incremental step-heating mineral ages from southeast Sri Lanka which suggest rapid intermediate (mid-crustal) cooling at 490–480 Ma, concurrent with Ordovician serpentinization and fluid flow in Sri Lanka (He *et al.* 2016), and orogenic collapse in adjacent east Antarctica and Mozambique (Jacobs *et al.* 2008). Our results link the end of prolonged HT deep-crustal orogenic metamorphism with the onset of rapid cooling associated with tectonic exhumation and continental stabilization.

2. Geologic setting

The Sri Lanka Precambrian 'pendant' consists of three larger and one smaller basement terranes (Cooray, 1994) distinguished on the basis of geologic and structural mapping (Kehelpannala, 2003,

2004) and Nd model ages (Milisenda *et al.* 1994; Kröner *et al.* 1991). A high-standing, central, dominantly supracrustal assemblage of granulite and UHT (>850 °C) metamorphic rocks (HC) is tectonically bounded on both sides by Neoproterozoic arc magmatic-dominated terrains metamorphosed to amphibolite and granulite facies (Fig. 2). The HC granulites experienced a major high-temperature (700–750 °C) folding and thrusting event that postdates peak metamorphism (Kleinschrodt, 1994). The western terrane boundary (separating the Wanni Complex, WC and the smaller Kadugannaw Complex, KC from the HC) is poorly defined and strongly overprinted (Voll & Kleinshcrodt, 1991), whereas the eastern terrane boundary is a well-defined thrust/shear contact (Voll & Kleinshcrodt, 1991; Kriegsman, 1995) referred to by He *et al.* (2016), and in this paper, as the 'eastern suture'.

The eastern suture is well-defined by a ca. 10–15 km wide thrust zone separating complexes with different metamorphic grades and Nd model ages (Voll & Kleinschrodt, 1991; Kriegsman, 1995). This 'tectonic mixed zone' (Ng *et al.* 2017), characterized by strong deformation, exotic tectonic slivers, migmatites, local serpentinite bodies, magnetite deposits and gold mineralization, is likely a major suture separating high-grade granulite/UHT rocks on the west (HC) from Grenville-age dominantly amphibolite facies granitoid and mafic orthogneisses on the east (VC; Santosh *et al.* 2014; He *et al.* 2016). West of the eastern suture, HC metamorphic pressures and temperatures broadly increase from 5–6 kb and ~700 °C in the northwest to 9–10 kb and ~830 °C in the southeast, near the eastern suture (Faulhaber & Raith, 1991; Schumacher & Faulhaber, 1994), suggesting the HC may be a tilted mid-to-lower-crustal section exhumed, in part, when the HC collided with the VC (Kehelpannala, 1997, 2003).

Similarities in lithology, geochemistry and geochronology of the western WC and eastern VC led Santosh *et al.* (2014) to interpret these bounding terranes as coeval magmatic arcs constructed above early to middle Neoproterozoic divergent subduction zones during closure of the Mozambique Ocean. In their model, the HC represents older trench fill sediments that were strongly deformed and metamorphosed via final ocean closure and collision of the arc terranes during assembly of Gondwana. More recently, He *et al.* (2016) document 920–970 Ma and 620–700 Ma subduction-related magmatism in the VC with no evidence for ages older than 1000 Ma, consistent with a continuous double subduction arc formation model (Li *et al.* 2024).

3. Timing and duration of HT metamorphism

Recent U-Pb zircon geochronology reveals widespread Pan-African medium- to high-grade metamorphism of all of the major Sri Lanka Proterozoic complexes. Granulite metamorphism of HC rocks occurred between 610 and 520 Ma (Kröner *et al.* 1987, 1994; Santosh *et al.* 2014; He *et al.* 2015, 2018) with peak metamorphism and charnockitization from 580–530 Ma (Dharmapriya *et al.* 2015, 2016; Takamura *et al.* 2015, 2016). Sajeev *et al.* (2010) interpret prograde UHT metamorphism in central Sri Lanka (western HC) to be ca. 570 Ma and retrograde UHT metamorphism to be ca. 550 Ma. Older 570 Ma zircon rim ages are interpreted to indicate partial melting prior to peak metamorphism and younger ca. 550 Ma zircon and monazite rim ages to indicate post-peak isothermal decompression at high pressures (Sajeev *et al.* 2010). Other recently reported U-Pb zircon metamorphic ages are no older than 590 Ma (Santosh *et al.* 2014; Ng *et al.* 2017; He *et al.* 2016, Dharmapriya *et al.* 2015).
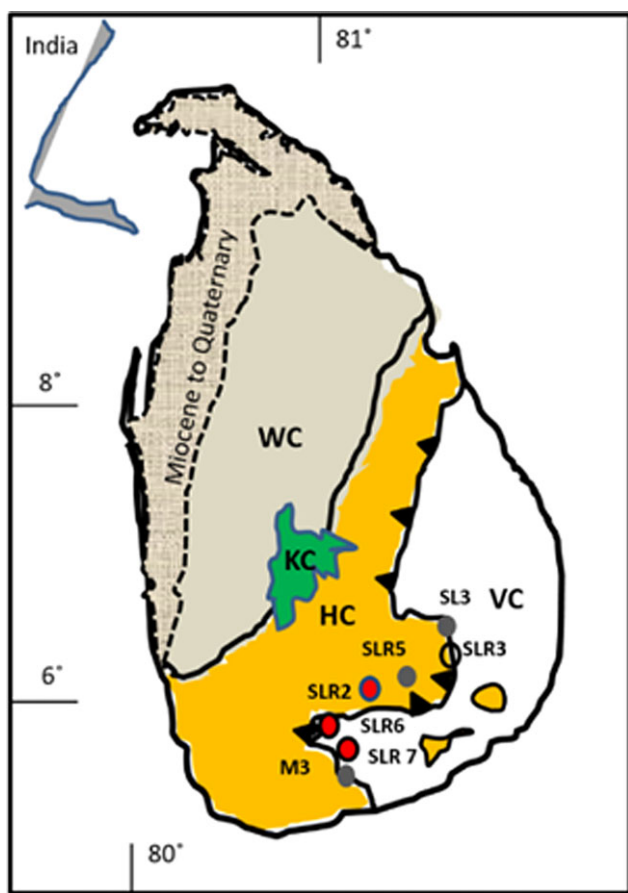
Figure 2. Tectonic map of Sri Lanka showing boundaries of crustal units delineated on the basis of Nd model ages (after Mathavan *et al.* 1998). WC = Wanni Complex; HC = Highland Complex; VC = Vijayan Complex, KC = Kadugannawa Complex. Shaded northwestern part of Sri Lanka represents Cenozoic sediments. Red symbols represent locations of ^{40}Ar-^{39}Ar ages, and grey symbols represent locations of monazite age data.

Felsic to mafic Neoproterozoic magmatic rocks in western Sri Lanka metamorphosed to upper amphibolite to granulite facies orthogneisses make up the dominant lithology of the western Wanni Complex. Lower intercept U-Pb zircon ages between 590 and 540 Ma likely represent the age of high-grade metamorphism (Hölzl *et al.* 1991). Charnockites and gneisses from Kurunegala (northwest Sri Lanka) yield a common regression line of ages with a lower intercept age of 563 Ma interpreted as the age of metamorphism (Baur *et al.* 1991). Until recently, the rocks of the VC have been less studied than the HC and WC rocks to the west because of political instability. The timing of granulite to amphibolite facies metamorphism of the VC, although less well constrained, was thought initially to be somewhat younger than the other terranes (between ~560 and 480 Ma; ; Hölzl *et al.* 1991, 1994; Cooray, 1994; Kröner & Williams, 1993). However, Kröner *et al.* (2013) documented that Neoproterozoic magmatic rocks (dated at 1062–935 Ma and 820–620 Ma; He *et al.* 2016; Ng *et al.* 2017) were regionally metamorphosed to upper amphibolite and granulite facies at ~580 Ma. More recent SIMS U-Pb zircon data yield metamorphic ages of ~580–521 Ma with charnockitization in the VC occurring at ~560 Ma (Ng *et al.* 2017) and He *et al.* (2016) report minor to significant Pb loss in the eastern suture at about 580–550 Ma.

Abundant high-precision SIMS and LA-ICPMS single grain and single spot zircon U-Pb ages in some sapphirine-bearing, pelitic and mafic granulites (Sajeev *et al.* 2007, 2010; Dharmapriya *et al.* 2015, 2016; Santosh *et al.* 2014; Osanai *et al.* 2016) yielded bimodal metamorphic age populations during the Ediacaran (620–580 Ma) and into the Cambrian (565–525 Ma), despite a lack of textural evidence for separate HT metamorphic events (Dharmapriya *et al.* 2017). Osanai *et al.* (2016) tied the bimodal metamorphic age populations in Sri Lanka temporally and spatially to separate 40 Ma duration UHT metamorphic episodes in southern Madagascar, southern India and East Antarctica during amalgamation of Gondwana during the Kuunga and East African Orogenies. More recently, a compilation of 1119 concordant zircon U-Pb ages from HC, together with LA-ICP-MS zircon U-Pb ages along with garnet/zircon REE data from HC (He *et al.* 2018) and SIMS U-Pb zircon ages from the VC (Ng *et al.* 2017) have been interpreted to indicate a single long-lived period (>50–100 Ma) of high-grade and UHT metamorphism lasting until ca. 520 Ma (and possibly until 480 Ma) associated with tectonic assembly of the Gondwana supercontinent.

4. Descriptions of dated bedrock samples

For this study, fifteen bedrock samples were collected from southeastern Sri Lanka near (<6 km) and within the eastern suture (Fig. 2; Table 1). From these, three samples of sheared gneiss within the suture (Fig. 3a), two samples of gneiss from the VC (Fig. 3b) and two gneiss samples from the HC (Fig. 3c and d) were selected for dating. Dated samples, briefly described below, include two garnet-biotite gneisses, a biotite gneiss, a garnet-sillimanite gneiss, a charnockitic gneiss, a garnet-bearing charnockitic gneiss and a garnet-hornblende gneiss (more detailed descriptions are available in Widanagamage (2011).

4.a. Highland Complex rocks

Garnet-sillimanite gneiss sample SLR5 exhibits subhedral, pinkish red, 1–5 mm garnet porphyroblasts in a matrix of sillimanite, feldspar, mica and quartz (Fig. 3d). Anastomosing centimetre-thick shear zones with flattened garnet porphyroblasts are also present. Garnet makes up 20–25% of the rock with coarse subhedral garnets surrounded by finer subhedral garnet over-growths. Sillimanite is abundant (30–40%) occurring both as inclusions in garnet and aligned in the foliation. Anhedral quartz (10–15%), subhedral plagioclase (5–10%), anhedral and K-feldspar (5%) make up the remainder of the rock.

Sample SLR2 is a medium-grained charnockitic gneiss. Fresh black and greyish-green samples consist of 10% biotite, 20% hypersthene, 10% hornblende, 10–15% plagioclase, 35–40% potassium feldspar and 10% quartz. Coarse euhedral to subhedral prismatic biotite crystals are aligned within the foliation and associated with subhedral, fractured hypersthene grains (Fig. 3e). Overall, the rock contains granoblastic texture with straight grain boundaries terminating at triple junctions.

Sample SL3 is a highly deformed garnet-biotite gneiss with sheared garnet porphyroblasts. Ribbon quartz (30–40%), biotite (20–30%) and aligned feldspars (40–50%) make up the bulk of the outcrop (Fig. 3a).

Sample M3 is a garnet-biotite gneiss with 1–2 mm diameter garnet porphyroblasts in a matrix of aligned biotite, quartz and feldspar. Subhedral quartz (25–30%), plagioclase (35–40%) and biotite (10–15%) make up the bulk of the outcrop.

Sample SLR3 is a white and red garnet-bearing hornblende gneiss collected from an outcrop of highly sheared rock within the

Table 1. Locations (UTM SL Grid_99 coordinate system) of samples, rock names and minerals dated

Location	Sample	E	N	Rock name	Mineral dated
Pareiyan ella	SL3	251430	183440	Hb-Bt gneiss	monazite
Hali Ela-Demodara road	SLR2	231492	189492	Charnockitic gneiss	biotite
Wellawaya	SLR3	234248	169578	Grt bearing Hb gneiss	hornblende
Rakwana Ganga	SLR5	192013	142643	Grt-Sil-gneiss	monazite
Walawe Ganga	SLR6	217991	135206	Grt charnockitic gneiss	biotite
Walawe Ganga	SLR7	214016	127665	Biotite gneiss	biotite
Walawe Ganga	M3	219173	113708	Grt-Bt gneiss	monazite

eastern suture. The gneiss is strongly foliated, consisting of mafic bands of coarse subhedral garnet and amphibole, and leucosomes of medium-grained quartz, plagioclase and perthitic feldspar (Fig. 3f).

4.b. Eastern suture rocks

Sample SL3 is a highly deformed garnet-biotite gneiss with sheared garnet porphyroblasts. Ribbon quartz (30–40%), biotite (20–30%) and aligned feldspars (40–50%) make up the bulk of the outcrop. (Fig. 3a)

Sample M3 is a garnet-biotite gneiss with 1–2 mm diameter garnet porphyroblasts in a matrix of aligned biotite, quartz and feldspar. Subhedral quartz (25–30%), plagioclase (35–40%) and biotite (10–15%) make up the bulk of the outcrop.

Sample SLR3 is a white and red garnet-bearing hornblende gneiss collected from an outcrop of highly sheared rock within the eastern suture. The gneiss is strongly foliated, consisting of mafic bands of coarse subhedral garnet and amphibole, and leucosomes of medium-grained quartz, plagioclase and perthitic feldspar (Fig. 3f).

4.c. Vijayan complex rocks

Sample SLR6 is a coarse-grained garnet-bearing charnockitic gneiss. Fresh surfaces are dark and light green with spots of red and black. Subhedral plagioclase (30–35%), subhedral hypersthene (20–25%), euhedral to subhedral prismatic biotite (10–15%), subhedral garnet (5–10%) and anhedral quartz (5–10%) make up the bulk of the rock (Fig. 3g). Granoblastic texture is common with polygonal quartz-feldspar associations.

Sample SLR7 is a white and black well-foliated biotite gneiss. Subhedral plagioclase (20–30%), anhedral quartz (10–15%), subhedral biotite (20–25%) and subhedral orthoclase (20–25%) make up the bulk of the rock. Minor alteration of biotite to chlorite and sericitization of feldspars is evident in thin section (Fig. 3h).

5. Analytical methods

5.a. EMP monazite geochronology

Monazite was dated in situ on thin sections (e.g. Williams *et al.* 1999) using a Cameca SX-100 electron microprobe at the New Mexico Bureau of Geology. Polished thin sections of samples were prepared, carbon coated and mapped for elements Si, Fe and Ce at an accelerating voltage of 15 kV, probe current of 200 nA and a beam size of 10 µm. Based on the Ce maps, monazite grains with a range of sizes and morphologies were identified and detailed Th, U,

Y and Pb maps of select grains were produced. Mapping was carried out at an accelerating voltage of 15 kV, probe current of 200 nA, using the PET crystal for analysis of Th and U; the TAP crystal for Y and a LPET crystal for Pb. Using the detailed chemical maps as a guide, major component analysis of the monazite grains was carried out, with attention focused on areas of grains with obviously different Th concentrations. These analyses included Ce, P, Si, Ca, Y, Th, La and a set of additional REE and were carried out at an accelerating voltage of 15 kV, and probe current of 20 nA.

Probe points were chosen using Th and Y maps to measure different chemical domains, and BSE images were used to avoid grain edges, fractures and holes to minimize non-uniform production of trace elemental X-rays. Background scans were run to fine-tune the background counting positions, in order to ensure accurate determination of trace concentrations. To determine the appropriate background levels for Th, Y, Pb and U, the data were processed in BK GII (Background II), a program developed by Mike Jercinovic (University of MA Amherst) that performs a regression analysis to determine background counting positions.

The monazites we analysed were typically 50–100 µm in diameter, large enough for choosing multiple probe points; two to nine points per grain were measured. Quantitative analysis of the Th, U, Y and Pb concentrations of monazite was done using the 'trace analysis' capabilities of the Cameca software. Many trace element analysis points were selected near points measured for major element data in order to ensure that trace concentrations were collected for Th, U, Pb and Y using the appropriate calibrations for the different chemical domains. Y was analysed with a TAP crystal, Th and U using a standard PET crystal, and Pb using a large PET crystal for better count rates. For these analyses, the Th (Mα) was calibrated using ThO2, Y (La) using a yttrium garnet, U (Mβ) using UO2 and Pb (Mα) using pyromorphite. Count times on peak were 300, 400, 400 and 600 seconds, respectively, using a probe current of 200 nA, and an accelerating voltage of 15 kV, yielding a visible beam size of around 3 µm and an effective excitation volume of probably closer to 5 µm in diameter. Calibration took place immediately prior to analysis with no intervening sample changes. The age equation was then solved using the Th, U and Pb concentrations for each analytical spot on monazite. Spot age errors were calculated by propagating the one sigma counting statistic error for Y, Th, U and Pb through the age equation, following the method provided by the **UThPbAge** spreadsheet developed by Gavril Săbău (2012). Before dates were accepted in the final dataset, the trace element analysis points, seen in the final BSE images, were compared to the trace concentrations to eliminate any disputable data.
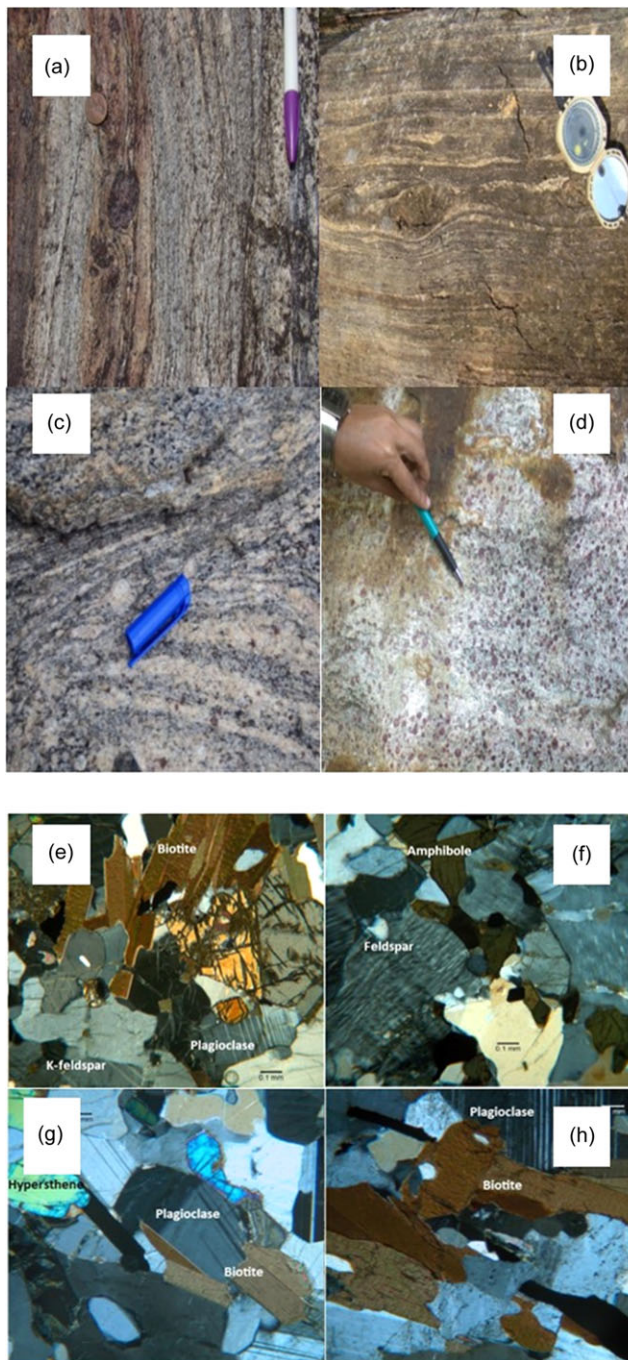
Figure 3. (top) Field photos of eastern suture (a), VC (b), and two HC gneisses (c, d). (bottom) Photomicrographs of samples dated via the ^{40}Ar-^{39}Ar method. e) SLR2 biotite, f) SLR3 hornblende, g) SLR6, biotite, h) SLR7 biotite.

5.b. 40Ar-39Ar thermochronology

Following standard mineral separation procedures, a minimum of 50 unaltered grains from each sample were hand-picked using a microscope. Samples were analysed at the New Mexico Geochronological Research Laboratory. Mineral separates of biotite and hornblende were loaded into aluminum discs and irradiated for 40 hours at the U.S. Geological Survey's TRIGA Reactor in Denver, Colorado. Neutron flux monitor of Fish Canyon Tuff sanidine (FC-2), with an assigned age of 28.02 Ma (Renne *et al.* 1998), was also irradiated with the samples. Argon

isotopes were measured using a Thermo-Fisher Scientific ARGUS VI mass spectrometer online with an automated all-metal extraction system. The mass spectrometer sensitivity is 1E-16 mol/fA. Samples were analysed using an incremental step-heating method by heating with a 75W Photon-Machine 810 nm diode laser. Released Ar gas was cleaned of reactive gases using a 1 SAES GP-50 getter operated at 450 ºC for five minutes. Mass spectrometer blanks and backgrounds were measured throughout the analysis, with total system blank and background of 25 ± 1%, 0.04 ± 20%, 0.05 ± 100%, 0.30 ± 85%, 0.10 ± 1.5%, x10−17 moles for masses of 40, 39, 38, 37 and 36, respectively. Through extrapolation of the sanidine flux monitor, neutron flux parameters, known as J-factors, were determined. These J-factors have a precision of ~±0.01% determined by analysing six individual crystals from each of four radial positions around the irradiation tray. K-glass and CaF2 were used to determine correction factors for interfering nuclear reactions. There corrections were $(^{40}Ar/^{39}Ar)_K = 0.008068 \pm 0.000068$, $(^{36}Ar/^{37}Ar)_{Ca} = 0.000273 \pm 0.0000002$ and $(^{39}Ar/^{37}Ar)_{Ca} = 0.000698 \pm 0.0000078$.

The uncertainty for individual dates for each heating step is reported at 1 sigma and reflects analytical measurement uncertainties that are corrected for system blank and detector calibrations. Reported cooling ages are inverse-variance weighted mean ages calculated from the selected heating steps and uncertainties are the square root of the sum of $1/\sigma^2$ values. When MSWD is greater than one, errors are multiplied by the square root of the MSWD. Nominal closure temperatures of 500 ºC for hornblende and 300 ºC for biotite are used (cf. McDougall and Harrison, 1999).

6. Results

6.a. Monazite EMP geochronology

Monazite grain sizes vary from 20 to 200 μm in diameter with most grains aligned and some elongate within the major rock fabric. Sixteen monazite grains were characterized and analysed in this study. Th concentration maps are presented in Fig. 4, and analytical data are recorded in Table 2.

6.a.1. Eastern suture ages

Five monazite grains were analysed from sample SL3 (Fig. 4). Four of the five grains show complex interior Th concentration textures with high Th rims that consistently yield younger spot ages (580–627 Ma). One grain with relatively uniform Th composition yielded an interior spot age of 598 Ma. Older core spot dates in these grains range from 667 Ma to 1868 Ma

Two monazite grains were analysed from sample M3 (Fig. 4). Grain 1 is round and contains a number of inclusions. Th concentration varies only slightly. One rim analysis gave an outlying young age of 541 Ma; all other ages are in the range of 595–671 Ma (15 spots total). Grain 2 is angular and elongate. Th concentration is relatively uniform. Seven spot ages range from 804 to 1031 Ma with no consistent variation in age from core to rim.

6.a.2. Highland Complex ages

Eight monazite grains were analysed from sample SLR5. One elongated grain with relatively uniform Th composition yielded an interior spot age of 589 Ma. The other seven grains vary from sub-rounded to angular to irregular and show complex to simple interior Th concentration textures and a few show clear rim
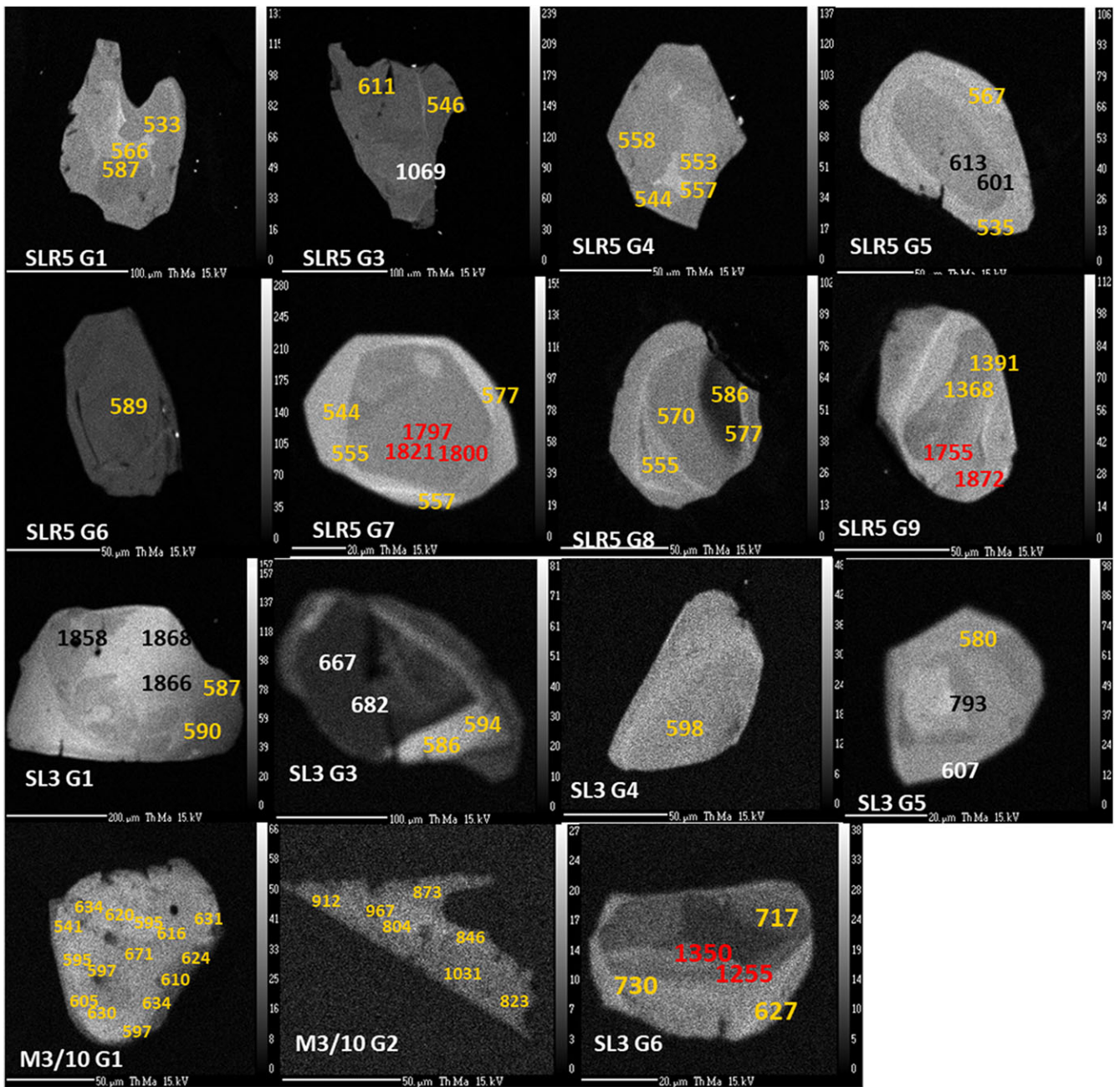
Figure 4. Th concentration maps of dated monazite grains from samples SL3, M3 and SLR5 with corresponding spot ages colour differentiated into younger and older age spots.

overgrowth textures. Four of the grains yield spot ages between 533 and 589 Ma and two yield similar rim ages with older core ages. One grain yielded only Proterozoic ages (1872–1368 Ma).

In summary, thirty spot ages from eight HC monazite grains reveal a dominance of Pan-African core and rim ages ranging from 533 Ma to 613 Ma (Fig. 5a) and forty spot ages from seven monazite grains from the eastern suture also preserve a dominance of Pan-African ages ranging from 541 Ma to 730 Ma (Fig. 5b). The two monazite age populations from the Highland Complex and the eastern suture are broadly consistent with one another except for the absence of 700–1000 Ma ages within the HC.

6.b. Chemical domains of dated monazite

The monazite age and textural data suggest that the Pan-African ages may result from chemical domains that formed during prograde and/or retrograde metamorphism (Foster *et al.* 2000). To better quantify this possible relation, chemical concentrations (Th, Y and U) in HC monazite grains (SLR5) and eastern suture rocks (SL3 and M3) were plotted with respect to spot ages and Th/U ratios were calculated and plotted against Y concentrations (Widanagamage, 2011). In the eastern suture, Pan-African dates represent primary metamorphic ages between 595 and 635 Ma.

Table 2. EMP total monazite age data from shear zones in HC-VC thrust boundary zone and HC southeastern Sri Lanka

Spot of Interest	Y (ppm)	Th (ppm)	U (ppm)	Pb (ppm)	Age, σ (Ma)
SL3 G1 S1	2230	79870	2550	2330	**587 ± 12**
SL3 G1 S2	2160	85790	2560	2500	**590 ± 14**
SL3 G1 S3	5420	80730	2800	7900	**1866 ± 30**
SL3 G1 S4	5510	85050	2870	8310	**1868 ± 25**
SL3 G1 S5	2360	69140	1720	6520	**1858 ± 32**
SL3 G3 S1	1970	7120	2770	490	**667 ± 32**
SL3 G3 S2	2000	5930	3210	510	**682 ± 32**
SL3 G3 S3	1990	45820	4060	1560	**586 ± 17**
SL3 G3 S4	2040	44550	4210	1560	**594 ± 17**
SL3 G4 S1	13200	14880	5520	890	**598 ± 22**
SL3 G5 S1	6320	38310	3270	1280	**580 ± 16**
SL3 G5 S2	6620	24300	2490	1170	**793 ± 24**
SL3 G5 S3	7740	37080	3080	1290	**607 ± 16**
SL3 G6 S1	1750	1490	860	280	**1350 ± 159**
SL3 G6 S2	1720	1430	990	280	**1255 ± 140**
SL3 G6 S3	12040	4300	4280	600	**717 ± 29**
SL3 G6 S4	4730	11970	3030	620	**627 ± 24**
SL3 G6 S5	6380	7720	2330	510	**730 ± 35**
M3-G1 S1	2320	29450	670	850	**597 ± 23**
M3-G1 S2	2290	27400	670	840	**630 ± 25**
M3-G1 S3	2330	26870	540	780	**605 ± 25**
M3-G1 S4	2370	24130	690	710	**597 ± 28**
M3-G1 S5	2360	18570	710	560	**595 ± 25**
M3-G1 S6	2140	10860	830	330	**541 ± 37**
M3-G1 S7	2520	23120	630	720	**634 ± 29**
M3-G1 S8	2200	25190	620	760	**620 ± 27**
M3-G1 S9	2280	31830	550	900	**595 ± 22**
M3-G1 S10	2240	29370	600	870	**616 ± 24**
M3-G1 S11	2350	24830	580	760	**631 ± 27**
M3-G1 S12	2530	23730	680	730	**624 ± 28**
M3-G1 S13	2430	24350	570	720	**610 ± 28**
M3-G1 S14	2380	21830	590	720	**671 ± 31**
M3-G1 S15	2380	22770	530	700	**634 ± 30**
M3-G2 S1	4440	4880	580	270	**873 ± 57**
M3-G2 S2	3640	7200	480	320	**804 ± 61**
M3-G2 S3	3670	5660	480	320	**967 ± 78**
M3-G2 S4	4570	4390	560	260	**912 ± 63**
M3-G2 S5	4090	5790	610	300	**846 ± 69**
M3-G2 S6	5130	3760	520	260	**1031 ± 77**
M3-G2 S7	5060	3770	640	220	**823 ± 63**
SRL5 G1 S1	2320	55240	7280	2090	**587 ± 13**
SRL5 G1 S2	6350	48920	6360	1670	**533 ± 14**
SRL5 G1 S3	2250	57080	6560	2000	**566 ± 13**

Table 2. (*Continued*)

Spot of Interest	Y (ppm)	Th (ppm)	U (ppm)	Pb (ppm)	Age, σ (Ma)
SRL5 G3 S1	2660	53040	6530	2050	611 ± 14
SRL5 G3 S2	6100	47600	6730	1710	546 ± 14
SRL5 G3 S3	2890	60670	6510	4040	1069 ± 20
SRL5 G4 S1	2110	66420	3020	1910	557 ± 13
SRL5 G4 S2	2210	61350	5190	1950	553 ± 13
SRL5 G4 S3	5920	46250	6740	1670	544 ± 14
SRL5 G4 S4	5670	47700	6830	1760	558 ± 14
SRL5 G5 S1	2690	50670	5350	1640	535 ± 14
SRL5 G5 S2	2440	52060	4080	1670	567 ± 15
SRL5 G5 S3	2480	40390	9520	1980	613 ± 14
SRL5 G5 S4	2530	40220	9580	1940	601 ± 14
SRL5 G6 S1	2310	45270	9420	2020	589 ± 13
SRL5 G7 S1	1930	70720	2630	1940	544 ± 13
SRL5 G7 S2	1910	70120	3040	2000	555 ± 13
SRL5 G7 S3	1760	85840	3040	2400	557 ± 11
SRL5 G7 S4	1760	81320	4670	2510	577 ± 13
SRL5 G7 S5	3080	57420	3820	5960	1797 ± 30
SRL5 G7 S6	3080	55730	3970	5950	1821 ± 30
SRL5 G7 S7	3080	56990	3780	5920	1800 ± 30
SRL5 G8 S1	5100	43490	7860	1730	555 ± 14
SRL5 G8 S2	5030	31730	12450	1860	570 ± 14
SRL5 G8 S3	4800	11420	12460	1360	577 ± 18
SRL5 G8 S4	4770	9570	12780	1360	586 ± 19
SRL5 G9 S1	2390	43220	6720	4200	1368 ± 25
SRL5 G9 S2	1730	33530	8520	5670	1872 ± 32
SRL5 G9 S3	1900	38230	11920	5130	1391 ± 24
SRL5 G9 S4	1790	32470	9720	5540	1755 ± 30
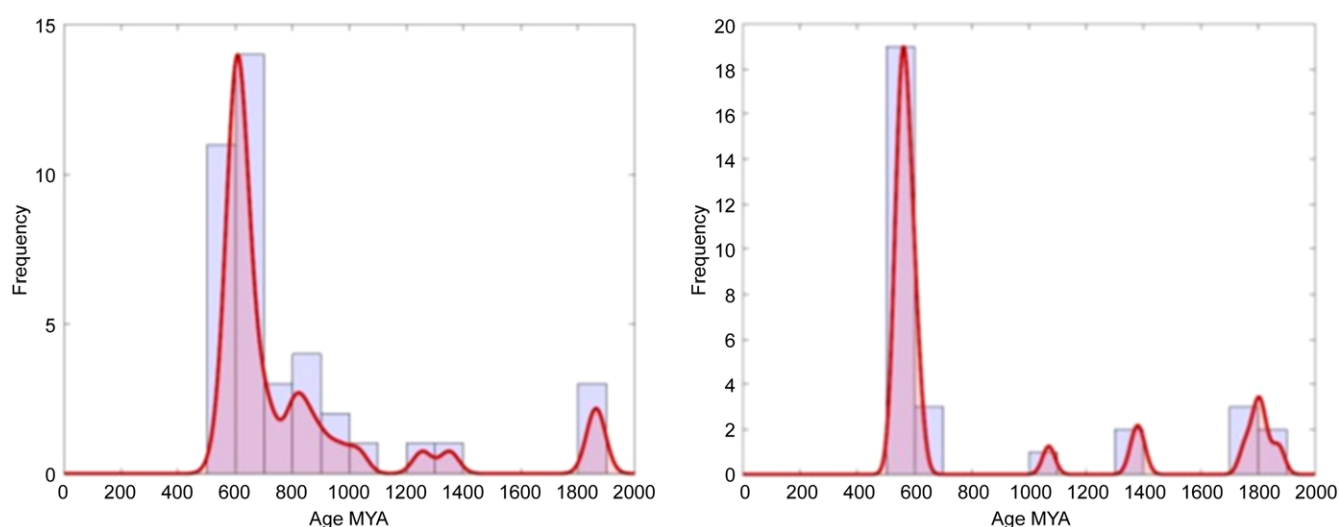
Figure 5. Age histograms showing probability curves for monazite spot ages from a) eastern suture (SL3, M3) and b) Highland Complex (SLR5).
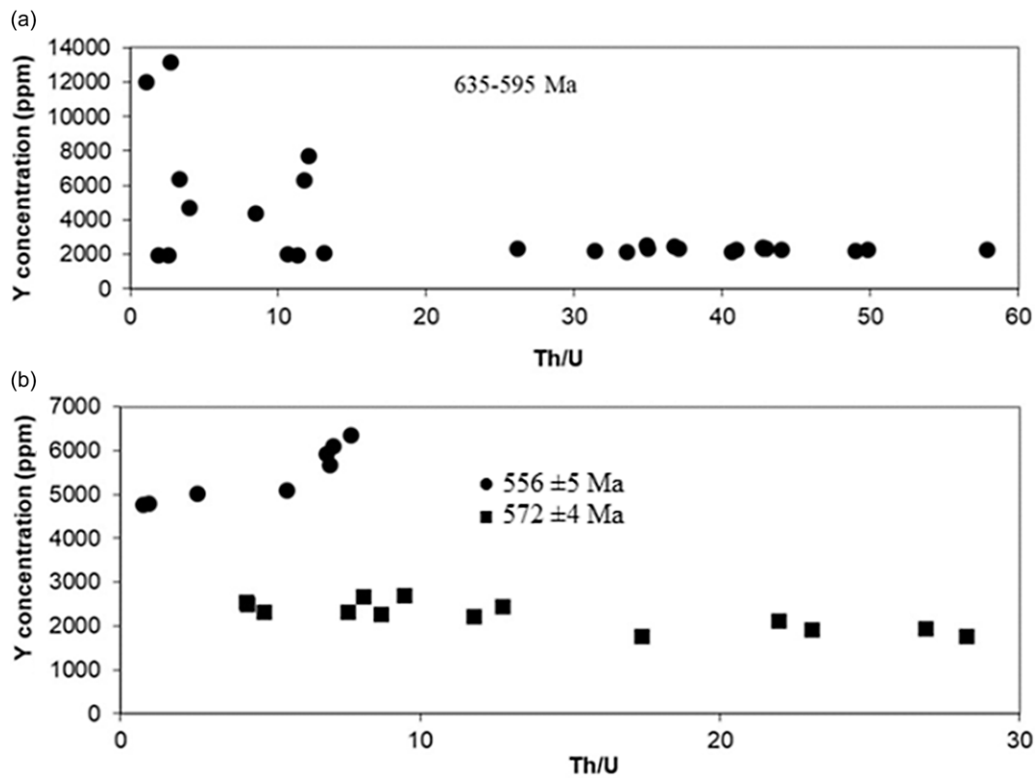
(a)

(b)

Figure 6. Plots of Y vs Th/U of Pan-African monazite spot ages. A – eastern suture (samples SL3 and M3); B – Highland Complex (sample SLR5).

Pan-African dates correspond to Y concentrations mostly near ~2000 ppm with a few spots having higher concentrations (up to 13000 ppm). The low Y spots show a large variation of Th/U (from 3 to 57), whereas higher Y spots have Th/U values of <12. No simple age-chemical correlation exists (Fig. 6a).

In the HC, Y concentrations of Pan-African spot ages align into two clusters: a low Y cluster (1500–2800 ppm) and a high Y cluster (4800–6200). Interestingly, the mean age for monazite spots with high Y concentrations is 556 ± 5 Ma, whereas the mean age for low Y concentration monazite spots is 572 ± 4 Ma. The older low Y Pan-African spot ages have a fairly wide range of Th/U ratios (4–30) whereas the younger high Y Pan-African spot ages have primarily lower and more restricted Th/U ratios varying in range from 2 to 7 (Fig. 6b).

6.c. ^{40}Ar-^{39}Ar thermochronology

The age spectra of the biotite and hornblende are shown in Figure 7 and analytical results presented in Table S (online Supplementary Material at http://journals.cambridge.org/geo). The age spectra are variably complex and weighted mean dates are calculated for segments of the spectra that are most uniform. Only one sample produced a plateau age that is defined by three consecutive steps comprising >50% of the total ^{39}Ar related. Despite this, the weighted mean and/or total gas ages for both hornblende and biotite grains yield internally consistent results and show that the minerals yield very similar cooling ages. We note that the cited high precision of the preferred ages does not reflect the geological uncertainty or the complexity of the age spectra, but rather is a consequence of the high analytical precision of the data. Thus, we do not attempt to over interpret individual cooling ages, but rather focus on the near concordance of mineral ages when discussing the overall cooling history of the region.

Hornblende from a garnet-rich hornblende gneiss collected within the eastern suture (sample SLR3) yielded a total gas age of 488.70 ± 0.06 Ma and produced a weighted mean age of 490.3 ± 0.1 Ma calculated from 38.4% of ^{39}Ar gas released from two consecutive steps. Biotite from HC charnockitic gneiss (sample SLR2) produced a preferred age of 478.12 ± 0.05 Ma calculated from 68.4% of ^{39}Ar gas released from two consecutive plateau steps and a total gas age of 479.14 ± 0.05 Ma. Biotite from a Vijayan Complex garnet-bearing charnockitic gneiss (sample SLR6) provided a preferred age of 488.1 ± 0.6 Ma calculated from 44.4% of ^{39}Ar released from two consecutive steps and a total gas age of 483.75 ± 0.07 Ma. Lastly, biotite from a Vijayan biotite gneiss (sample SLR7) produced a weighted mean age of 477.76 ± 0.53 Ma calculated from 63.9% of the ^{39}Ar released from seven consecutive steps and total gas age of 472.68 ± 0.05 Ma.

In summary, all four ^{40}Ar-^{39}Ar mineral ages within and near the eastern suture yielded nearly concordant biotite and hornblende ages between 478 and 490 Ma.

7. Discussion

U-Pb zircon geochronology on UHT metapelites and mafic granulite from the western HC (central Sri Lanka) document late Neoproterozoic 580–530 Ma metamorphism associated with final assembly of Gondwana. Our EMP monazite study of the eastern suture region similarly yields a dominance of 600–500 Ma ages in newly grown metamorphic monazite grains and from metamorphic monazite rim overgrowths surrounding Proterozoic-aged cores. The Proterozoic core ages obtained here are consistent with derivation from magmatic protoliths of Palaeoproterozoic, Mesoproterozoic and Neoproterozoic sources determined from U-Pb detrital zircon ages in the HC (Kitano *et al.* 2018; Takamura *et al.* 2016). The middle Neoproterozoic monazite ages from
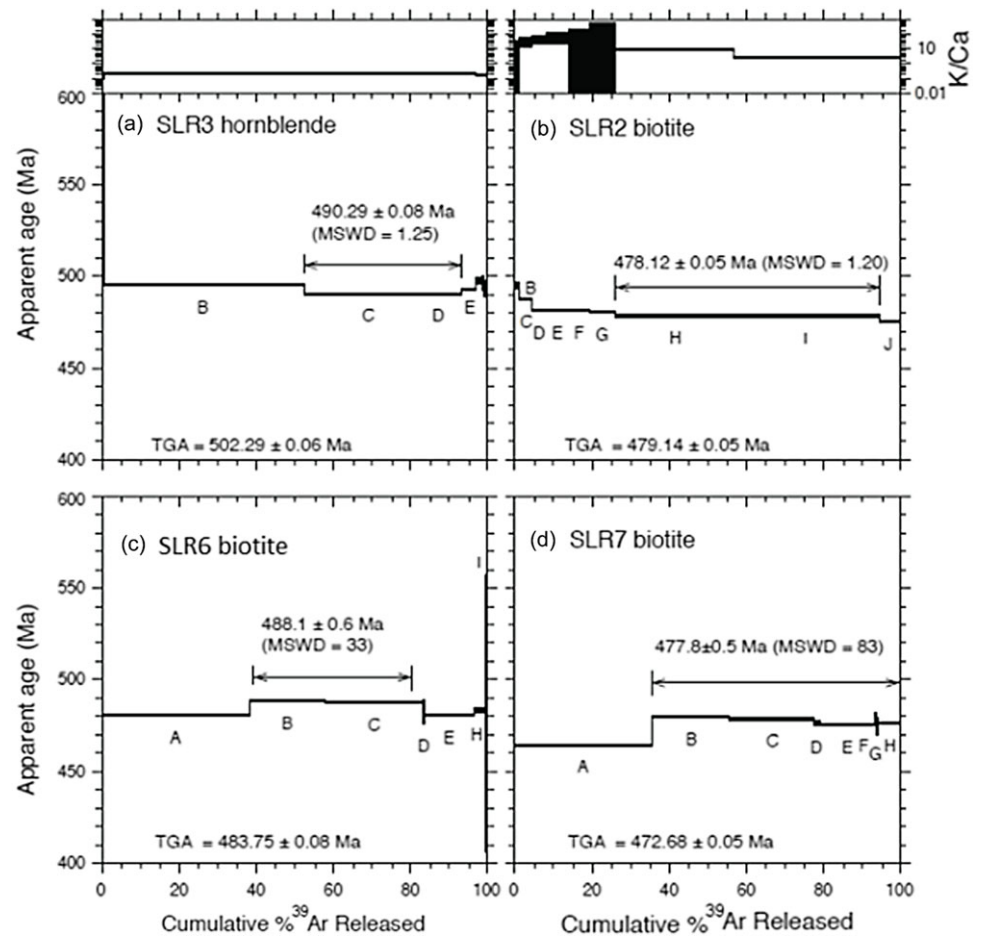
Figure 7. ^{40}Ar-^{39}Ar release spectra. (a) Hornblende from the eastern suture, (b) biotite from the HC, (c) and (d) biotite from the VC.

eastern suture rocks may have come from the western peripheral region of the Vijayan complex itself (Ng *et al.* 2017).

Yttrium content of monazite depends heavily on reactions involving garnet (Kohn *et al.* 2005). Y tends to be sequestered during prograde metamorphism as garnet grows and is released during retrograde reactions that consume garnet (Högdahl *et al.* 2011). Our slightly younger, high Y monazite spot ages are consistent with the HC reaching peak metamorphism (M1) at 572 ± 4 Ma followed by lower-crustal near isothermal decompression during retrogression (M2) at 556 ± 5 Ma. In their study of select UHT granulites from the western margin of the HC (central Sri Lanka), Sajeev *et al.* (2010) obtained similar Proterozoic SHRIMP U-Pb ages from zircon cores and monazite grains with overgrowths dated at 569 ± 7 Ma and 551 ± 7 Ma (Fig. 8). They interpreted the ca. 570 Ma overgrowths as the age of prograde (M1) metamorphism and the younger ca. 550 Ma overgrowths as the time of retrograde (M2) metamorphism during decompression. Their textural work suggests that early garnet growth during peak metamorphism was followed by garnet consumption during decompression, similar to our interpretation based on chemical age analysis of uniform and textured monazite grains of similar spot ages. The timing of peak and retrograde HC metamorphism obtained in this study and by Sajeev *et al.* (2010) are remarkably similar despite the use of different techniques (EMP and SHRIMP) and sample localities that are ca. 50–70 km apart (Fig. 8).

Few intermediate-temperature (500–300 °C) mid-crustal cooling ages of high-grade Sri Lankan basement rocks exist. A dozen Rb-Sr biotite ages reported in Hölzl *et al.* (1991) scatter around
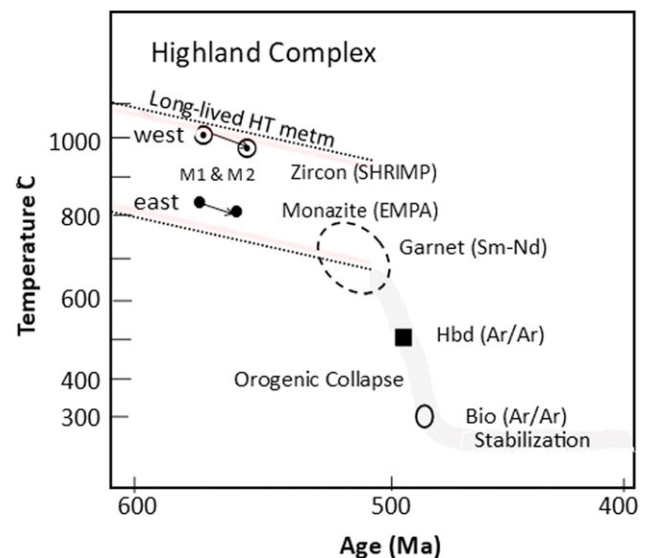

Figure 8. Schematic T-t diagram of long-lived HT orogenic metamorphism followed by rapid early Ordovician deep to mid-crustal exhumation and stabilization, HC, Sri Lanka.

470–440 Ma, indicating the time of cooling through a single closure temperature. Interestingly, very large gemstone-quality detrital zircons from sedimentary deposits within the HC (Nasdala *et al.*

2004) yielded Late Ordovician zircon (U-Th)/He ages which scatter around 443±9 Ma, which is consistent with both Rb-Sr biotite and (U-Th)/He in very large zircons having similar effective closure temperatures of about 250–300 °C (Nasdala *et al.* 2004).

Our new ^{40}Ar-^{39}Ar mineral age data from different minerals with significantly different closure temperatures (~500 °C for hornblende and ~300 °C for biotite) suggest rapid cooling from above 500 °C to below 300 °C during the Ordovician (at 478–490 Ma; Fig. 8). Braun and Kriegsman (2003) tentatively suggested that Ordovician cooling of the HC may have been related to thrusting of the HC atop the VC. However, our results indicate that both the HC and the VC rocks, as well as the intervening suture rocks all cooled simultaneously, suggesting cooling after, or at the end of, thrusting.

7.a. Linking high and intermediate-temperature thermal histories

A prolonged period of slow high-temperature cooling of Sri Lanka rocks has been argued for, in part, on the basis of modelling of retrograde diffusion zoning in garnet dated at 550–480 Ma (Sm-Nd ages; Hölzl *et al.* 1991; Fig. 8). Petrologic modelling by Fernando *et al.* (2003) suggests slow high-T cooling (1–5 °C /Ma) during which garnet diffusion is fast and homogeneously reset. They interpreted ongoing slow cooling at 1–5 °C /Ma to simply reflect slow ascent via low erosion rates associated with isostatic rebound, with final cooling through 300 °C at ~440 Ma (based on Rb-Sr biotite ages of Hölzl *et al.* 1991). Our new ^{40}Ar-^{39}Ar mineral age results instead suggest rapid cooling was simultaneous with the cessation of both high-T zircon growth (He *et al.* 2018) and garnet growth (Hölzl *et al.* 1991), and more likely reflects rapid exhumation associated with tectonic-driven uplift, not slow isostatic rebound.

Geologic evidence for rapid mid-crustal exhumation causing accelerated cooling comes from the widespread existence of garnet decomposition textures throughout the HC (Schumacher & Faulhaber, 1994), by aluminous metapelites with localized late-stage andalusite (Hiroi *et al.* 1994; Raase & Schenk, 1994) and by local pyrophyllite rims around sillimanite (grown at T <400 °C; Dharmapriya *et al.* 2017). Additionally, Hiroi *et al.* (2014) documented quench textures of felsite inclusions (within garnet) in lower-crustal HC granulites which they interpreted as features associated with fast exhumation of lower-crustal rocks to andalusite stable upper-crustal conditions during continental collision. Beyond these features, there is no petrological evidence that the bedrock of Sri Lanka experienced any widespread low-grade metamorphism after rapid exhumation of HT rocks to the mid-crust. Young brittle upper-crustal faults dated using low-temperature thermochronology (zircon, apatite fission track and U-Th-Sm)/He analyses indicate two main shallow-level exhumation stages at 260–140 Ma and 90±20 Ma related to regional episodes of Gondwana break-up (Emmel *et al.* 2012). Additionally, ca. 40 Ma zircon fission track ages from Sri Lanka (reported by Garver, 2002) may document onset of the most recent shallow-level exhumation leaving Sri Lanka as one of the highest stable regions in the world (Emmel *et al.* 2012).

7.b. Regional collapse, cooling, and stabilization

Although our new ^{40}Ar-^{39}Ar 490–480 Ma mineral ages are from only southeastern Sri Lanka near and within the eastern suture, initial thermochronologic mineral ages published in the last century hint at its probable regional extent. Early K-Ar biotite ages

scattered throughout Sri Lanka are between 550–450 Ma (Cooray, 1969) and Rb-Sr mineral ages (12 biotite and one hornblende are 490–440 Ma (Hölzl *et al.* 1991; Burton & O'Nions, 1990). Additionally, unpublished ages from multiple minerals in a single rock vary from ca. 500–420 Ma (Irwin *et al.* 1987). While poorly constrained overall, the lack of K-Ar and Rb-Sr mineral ages younger than 420 Ma from these early thermochronologic datasets seems to suggest regional rapid cooling of Sri Lanka in the early Ordovician with limited to no younger intermediate-temperature cooling or reheating since that time.

He *et al.* (2016) document early Ordovician (ca. 485 Ma) serpentinite derived from metasomatism of ultramafic magmas along the eastern suture in southern Sri Lanka, noting similar aged serpentinites in southern India and southern Madagascar (on the basis of K-Ar phlogopite ages; Rajesh *et al.* 2004; Rakotondrazafy *et al.* 1997). He *et al.* (2016) argue that zircon growth may have occurred during metasomatism related to serpentinization, and may, therefore, post-date crystallization of the ultramafic rocks themselves. If so, it seems that widespread rapid cooling of much of Sri Lanka at ca. 490–480 Ma was concurrent with significant fluidization along the eastern suture after the HC and VC complexes were juxtaposed and metamorphosed (ca. 600–500 Ma). Malaviarachchi & Takasu (2011) similarly argue for Ordovician fluidization along fractures at 460–480 Ma on the basis of CHIME monazite ages within apparent mesh-like zone fractures within monazite.

Rapid Ordovician exhumation following long-lived high-temperature metamorphism is best interpreted in the context of Sri Lanka's location within the heart of Gondwana. Indeed, early Palaeozoic orogenic collapse of similar age has been proposed for nearby correlated regions of Gondwana including Dronning Maud Land (DML) and Mozambique (Fig. 1; Jacobs *et al.* 2008). Synchronous extensional shearing and granitoid intrusion at 520–485 Ma in those regions is attributed to partial delamination of the orogenic root formed in the interior of Gondwana at the end of supercontinent assembly. Although such late features are largely absent in Sri Lanka, minor late (514 ± 3 Ma) melt crystallization has been documented in the HC by Dharmapriya *et al.* (2017), and the lack of late overprinting collapse structures (i.e. extensional shear zones) could reflect a more deeply exposed level of collapsed crust in Sri Lanka.

8. Conclusions

New 635–595 Ma EMP Chemical Th-U-Pb dates of monazite recorded from rocks within the eastern suture likely formed during shearing at moderate P-T conditions and may, therefore, date the initial juxtaposition of the HC and VC complexes. Ca. 600 Ma arc collision and crustal thickening may have led to a prolonged period of HT metamorphism of much of the HC. Metamorphism which peaked in the eastern HC at 570 Ma was followed by retrogression of these rocks beginning at ca. 560 Ma. Our somewhat older retrogression age from the easternmost HC compared to the western HC (ca. 550 Ma; Sajeev *et al.* 2010) might indicate earlier onset of exhumation of the deepest eastern HC rocks compared to the western HC. Our new EMP monazite dating results compare well with prior U-Pb zircon geochronologic results (compiled by He *et al.* 2018) which suggest that widespread HT metamorphism in the HC was long duration and persisted until at least 520 Ma and possibly until 480 Ma.

Concordant ^{40}Ar-^{39}Ar mineral ages indicate cooling from above ca. 500 °C to below ca. 300 °C of both the HC and VC rocks

in southeastern Sri Lanka occurred ca. 490–480 Ma, 30–40 Ma earlier than initially interpreted based on Rb-Sr biotite ages (Hölzl *et al.* 1991). The cessation of long-lived (>50–100 Ma) HT metamorphism is therefore linked temporally to rapid intermediate-temperature cooling. Fast exhumation-related cooling also occurred simultaneously with region-wide serpentinization of ultramafic plutons tectonically emplaced during construction of Gondwana (He *et al.* 2016; Rajesh *et al.* 2004; Rakotondrazafy *et al.* 1997). Rapid lower to mid-crustal cooling and associated metasomatism would be expected during collapse of hot over-thickened orogenic Gondwana crust as has been proposed in nearby (at that time) southern India (Rajeesh *et al.* 2006), perhaps facilitated by channel flow (Hiroi *et al.* 2014).

Orogenic collapse is well documented in areas of over-thickened crust, both young and old, and has been viewed as a critical step in the stabilization of continents (Holm *et al.* 1998; Nelson, 1991). Ordovician orogenic collapse of Sri Lanka and its surrounding regions (east Antarctica and Mozambique) after Gondwana assembly is interpreted to reflect the time and process by which this part of Gondwana was stabilized. The absence of late Cambrian-early Ordovician extensional collapse structures and late-tectonic magmatism compared to surrounding regions may simply reflect exposure of more deeply exhumed collapsed crust preserved in Sri Lanka.

References

Baur N, Kröner A, Todt W, Liew TC and Hofmann AW (1991) U-Pb isotopic systematics of zircons from prograde and retrograde transition zones in high grade orthogneisses, Sri Lanka. *Journal of Geology* **99**, 527–545.

Braun I and Kriegsman LM (2003) Proterozoic crustal evolution of southernmost India and Sri Lanka. *Geological Society, London, Special Publications* **206**, 169–202.

Burton KW and O'Nions RK (1990) The timescale and mechanism of granulite formation at Kurunegala, Sri Lanka. *Contributions to Mineralogy and Petrology* **106**, 66–89.

Cooray PG (1969) The significance of mica ages from the crystalline rocks of Ceylon. In *Age Relations in High-grade Metamorphic Terrains*, pp. 47–56. Geological Association, Canada, Special Paper 5.

Cooray PG (1994) The Precambrian of Sri Lanka: a historical view. *Precambrian Research* **66**, 3–18.

Dharmapriya PL, Malaviarachchi SPK, Santosh M and Tang L (2015) Late-Neoproterozoic ultrahigh-temperature metamorphism in the Highland Complex, Sri Lanka. *Precambrian Research* **271**, 311–333.

Dharmapriya PL, Malaviarachchi SPK, Sajeev K and Zhang C (2016) New LA-ICPMS U-Pb ages of detrital zircons from the Highland Complex: insights into late Cryogenian to early Cambrian (ca. 665–535 Ma) linkage between Sri Lanka and India. *International Geology Review* **58**, 1856–1883.

Dharmapriya PL, Malaviarachchi SPK, Kriegsman LM, Galli A, Sajeev K and Zhang C (2017) New constraints on the P-T path of HT/UHT metapelites from the highland complex of Sri Lanka. *Geoscience Frontiers* **8**, 1405–1430.

Emmel B, Lisker F and Hewawasam T (2012) Thermochronological dating of brittle structures in basement rocks: a case study from the onshore passive margin of SW Sri Lanka. *Journal of Geophysical Research* **117**, B10407.

Faulhaber S and Raith M (1991) Geothermometry and geobarometry of high-grade rocks: a case study of garnet pyroxene granulites in southern Sri Lanka. *Mineralogical Magazine* **55**, 33–56.

Fernando GWAR, Hauzenberger CA, Baumgartner LP and Hofmeister W (2003) Modeling of retrograde diffusion zoning in garnet: evidence for slow cooling of granulates from the Highland complex of Sri Lanka. *Mineralogy and Petrology* **78**, 53–71.

Fitzsimmons ICW (2016) Pan-African granulites of Madagascar and southern India: Gondwana assembly and parallels with modern Tibet. *Journal of Mineralogical and Petrological Sciences* **111**, 73–88.

Foster G, Kinny P, Vance D, Prince CI and Harris N (2000) The significance of monazite U-Th-Pb age data in metamorphic assemblages; a combined study of monazite and garnet chronometry. *Earth and Planetary Science Letters* **181**, 327–340.

Garver JI (2002) Discussion: "Metamictization of natural zircon: accumulation vs. thermal annealing of radioactivity-induced damage" by Nasdala *et al.*, 2001. *Contributions to Mineralogy & Petrology* **143**, 756–757.

He X-F, Santosh M, Tsunogae T and Malaviarachchi S (2015) Early to late Neoproterozoic magmatism and magma mixing-mingling in Sri Lanka: implications for convergent margin processes during Gondwana assembly. *Gondwana Research* **32**, 151–180.

He X-F, Santosh M, Tsunogae T, Malaviarachchi S and Dharmapriya PL (2016) Neoproterozoic arc accretion along the 'eastern suture' in Sri Lanka during Gondwana assembly. *Precambrian Research* **279**, 57–80.

He X-F, Hand M, Santosh M, Kelsey DE, Morrissey LJ and Tsunogae T (2018) Long-lived metamorphic P-T-t evolution of the Highland Complex, Sri Lanka: Insights from mafic granulites. *Precambrian Research* **316**, 227–243.

Hiroi Y, Ogo Y and Namba K (1994) Evidence for prograde metamorphic evolution of Sri Lankan pelitic granulites, and implications for the development of continental crust. *Precambrian Research* **66**, 245–263.

Hiroi Y, Yanagi A, Kato M, Kobayashi T, Prame B, Hokada T, Satish-Kumar M, Ishikawa M, Adachi T, Osanai Y, Motoyoshi Y and Shiraishi K (2014) Supercooled melt inclusions in lower-crustal granulites as a consequence of rapid exhumation by channel flow. *Gondwana Research* **25**, 226–234.

Högdahl K, Majka J, Sjostrom H, Nilsson K, Claesson S and Konečný P (2011) Reactive monazite and robust zircon growth in diatexites and leucogranites from a hot, slowly cooled orogeny: implications for the Paleoproterozoic tectonic evolution of the central Fennoscandian Shield, Sweden. *Contributions to Mineralogy and Petrology* **163**, 167–188.

Hölzl S, Hofmann AW, Todt W and Kohler H (1994) U-Pb Geochronology of the Sri Lankan basement. *Precambrian Research* **66**, 123–149.

Hölzl S, Kohler H, Kröner A, Jaeckel P and Liew TC (1991) Geochronology of the Sri Lankan basement. In *The Crystalline Crust of Sri Lanka. Part I, Summary of Research of the German-Sri Lankan Consortium: Professional Paper no. 5* (eds A Kröner), pp. 237–253. Sri Lanka: Geological Survey Department.

Holm D, Darrah KS and Lux DR (1998) Evidence for widespread ~1760 Ma metamorphism and rapid crustal stabilization of the early Proterozoic (1870–1820 Ma) Penokean orogen, Minnesota. *American Journal of Science* **298**, 60–81.

Holm D, Medaris LG, McDannell KT, Schneider DA, Schulz K, Singer BS and Jicha BR (2020) Growth, overprinting, and stabilization of Proterozoic provinces in the southern Lake Superior region. *Precambrian Research* **339**, 1–12.

Irwin JJ, Kirschbaum C, Lim T, Glassley W, Ryerson FJ, Shaw HF, Niemeyer S and Abeysinghe PB (1987) Laser-microprobe ^{40}Ar-^{39}Ar ages of high-grade metamorphic rock from Sri Lanka. *Eos* **68**, 431.

Jacobs J, Bingen B, Thomas RJ, Buer W, Wingate MTD and Feitio P (2008) Early Paleozoic orogenic collapse and voluminous late-tectonic magmatism in Dronning Maud Land and Mozambique: insights into the partially delaminated orogenic root of the East African-Antarctic Orogen? *Geological Society, London, Special Publications* **308**, 69–90.

Jöns N and Schenk V (2011) The ultrahigh temperature granulites of southern Madagascar in a polymetamorphic context: implications for the amalgamation of the Gondwana supercontinent. *European Journal of Mineralogy* **23**, 127–156.

Kehelpannala KVW (1997) Deformation of high grade Gondwana fragments; Sri Lanka. *Gondwana Research* **1**, 47–68.

Kehelpannala KVW (2003) Structural evolution of the middle to lower crust in Sri Lanka- a review. *Journal of the Geological Society of Sri Lanka* **11**, 45–85.

Kehelpannala KVW (2004) Arc Accretion around Sri Lanka during the assembly of Gondwana. *Gondwana Research* **7**, 41–46.

Kitano I, Osanai Y, Nakano N, Adachi T and Fitzsimons ICW (2018) Detrital zircon and igneous protolith ages of high-grade metamorphic rocks in the Highland and Wanni Complexes, Sri Lanka: Their geochronological correlation with southern India and East Antarctica. *Journal of Asian Earth Sciences* **156**, 122–144.

Kleinschrodt R (1994) Large scale thrusting in the lower crustal basement of Sri Lanka. *Precambrian Research* **66**, 39–57.

Kohn MJ, Wieland MS, Parkinson CD and Upreti BN (2005) Five generations of monazite in Langtang gneisses: implications for chronology of the Himalayan metamorphic core. *Journal of Metamorphic Geology* **23**, 399–406.

Kriegsman L (1995) The Pan African events in East Antarctica: a review from Sri Lanka and the Mozambique Belt. *Precambrian Research* **75**, 263–277.

Kröner A, Cooray PG and Vitanage PW (1991) Lithotectonic subdivision of the Precambrian basement in Sri Lanka. In *The Crystalline Crust of Sri Lanka. Part I, Summary of Research of the German-Sri Lankan Consortium: Professional Paper no. 5* (eds A Kröner), pp. 5–21. Sri Lanka: Geological Survey Department.

Kröner A and Williams IS (1993) Age of metamorphism in the high-grade rocks of Sri Lanka. *Journal of Geology* **101**, 513–521.

Kröner A, Jaeckel P and Williams IS (1994) Pb-loss patterns in zircons from a high-grade metamorphic terrain as revealed by different dating methods: U-Pb and Pb-Pb ages for igneous and metamorphic zircons from northern Sri Lanka. *Precambrian Research* **66**, 151–181.

Kröner A, Williams IS, Compston W, Baur N, Vitanage PW and Perera LRK (1987) Zircon ion microprobe dating of high-grade rocks in Sri Lanka. *Journal of Geology* **95**, 775–791.

Kröner A, Rojas-Agramonte Y, Kehelpannala KVW, Zack T, Hegner E, Geng H-Y, Wong JP-M and Barth M (2013) Age, Nd-Hf isotopes, and geochemistry of the Vijayan Complex of eastern and southern Sri Lanka: a Grenville-age magmatic arc of unknown derivation. *Precambrian Research* **234**, 288–321.

Lawver LA, Gahagan LM and Dalziel IWD (1998) A tight-fit early Mesozoic Gondwana, a plate reconstruction perspective. *Memoirs of National Institute of Polar Research, Tokyo* **53**, 214–229.

Li L-S, Capitanio FA, Cawood PA, Wu B-J, Zhai M-G and Wang X-L (2024) Double subduction controls on long-lived continental tectonics and subcontinental mantle temperatures. *Geology* **52**, 836–840.

Malaviarachchi S and Takasu A (2011) Electron microprobe dating of Monazites from Sri Lanka: implications on multiple thermal events related to Gondwana. *Journal of the Geological Society of Sri Lanka* **14**, 81–90.

Mathavan V, Prame WKBN and Cooray PG (1998) Geology of the high-grade Proterozoic terrains of Sri Lanka and the assembly of Gondwana: an update on recent developments. *Gondwana Research* **2**, 237–250.

McDougall I and Harrison TM (1999) *Geochronology and Thermochronology by the 40Ar-39Ar Method, Second ed*. New York: Oxford Univ. Press.

Milisenda CC, Liew TC, Hofmann AW and Kröner A (1994) Nd isotopic mapping of the Sri Lanka basement: update, and additional constraints from Sr. isotopes. *Precambrian Research* **66**, 95–110.

Nelson KD (1991) A unified view of craton evolution motivated by recent deep seismic reflection and refraction results. *Geophysical Journal International* **105**, 25–30.

Plavsa D, Collins AS, Payne JL, Foden JD, Clark C and Santosh M (2014) Detrital zircons in basement metasedimentary protoliths unveil the origins of southern India. *Bulletin of the Geological Society of America* **126**, 791–811.

Nasdala L, Reiners PW, Garver JI, Kennedy AK, Stern RA, Balan E and Wirth R (2004) Incomplete retention of radiation damage in zircon from Sri Lanka. *American Mineralogist* **89**, 210–231.

Ng SW-P, Whitehouse MJ, Tam TP-K, Jayasingha P, Wong JP-M, Denyszyn SW, Yiu JS-Y and Chang S-C (2017) Ca. 820–640 Ma SIMS U-Pb age signal in the peripheral Vijayan Complex, Sri Lanka: Identifying magmatic pulses in the assembly of Gondwana. *Precambrian Research* **294**, 244–256.

Osanai Y, Sajeev K, Nakano N, Kitano I, Kehelpannala WKV, Kato R, Adachi T and Malaviarachchi SPK (2016) UHT granulites of the Highland Complex, Sri. Lanka II: geochronological constraints and implication for Gondwana correlation. *Journal of Mineralogical and Petrological Sciences* **111**, 157–169.

Raase R and Schenk V (1994) Petrology of granulite facies metapelites of highland complex of Sri Lanka: implications for metamorphic zonation and P-T path. *Precambrian Research* **66**, 265–294.

Rajesh RJ, Arima M and Santosh M (2004) Dunite, glimmerite, and spinellite in Achankovil Shear Zone, South India: Implications for highly potassic CO_2-rich melt influx along an intra-continental shear zone. *Gondwana Research* **7**, 961–974.

Rajeesh RJ, Yokoyama K, Santosh M, Arai S, Oh CW and Kim SW (2006) Zirconolite and baddeleyite in an ultramafic suite from Southern India: early ordovician carbonatite-type melts associated with extensional collapse of the Gondwana crust. *Journal of Geology* **114**, 171–188.

Rakotondrazafy R, Pierdzig S, Raith MM and Hoernes S (1997) Phlogopite-mineralizations in the Beraketa belt of southern Madagascar: a spectacular example of channelized fluid flow and fluid-rock interaction. *Gondwana Research* **5**, 81–82.

Renne PR, Swisher CC, Deino AL, Karner DB, Owens TL and DePaolo DJ (1998) Intercalibration of standards, absolute ages and uncertainties in ^{40}Ar-^{39}Ar dating. *Chemical Geology* **145**, 117–152.

Săbău G (2012) Chemical U-Th-Pb Geochronology: a precise explicit approximation of the age equation and associated errors. *Geochronometria* **39**, 167–179.

Sajeev K, Osanai Y, Connolly JAD, Suzuki S, Ishioka J, Kagami H and Rino S (2007) Extreme crustal metamorphism during a Neoproterozoic event in Sri Lanka: a study of dry mafic granulites. *Journal of Geology* **115**, 563–582.

Sajeev K, Williams IS and Osani Y (2010) Sensitive high-resolution ion microprobe U-Pb dating of prograde and retrograde ultrahigh-temperature metamorphism as exemplified by Sri Lankan granulites. *Geology* **38**, 971–974.

Santosh M, Tsunogae T, Malaviarachchi S, Zhang Z, Ding H, Tang L and Dharmapriya PL (2014) Neoproterozoic crustal evolution in Sri Lanka: insight from petrologic, geochemical and zircon U-Pb and Lu-Hf isotopic data and implication for Gondwana assembly. *Precambrian Research* **255**, 1–29.

Schumacher R and Faulhaber S (1994) Summary and Discussion of P-T estimates from garnet-pyroxene-plagioclase-quartz-bearing granulite-facies rocks from Sri Lanka: *Precambrian Research* **66**, 295–308.

Shiraishi K, Ellis DJ, Hiroi Y, Fanning CM, Motoyoshi Y and Nakai Y (1994) Cambrian Orogenic Belt in east Gondwana and Sri Lanka: Terrane assembly in Pan African lower crust. *Journal of Geology* **102**, 47–65.

Takamura Y, Tsunogae T, Santosh M, Malaviarachchi S and Tsutsumi Y (2015) Petrology and zircon U-Pb geochronology of metagabbro from the Highland Complex, Sri Lanka: implications for the correlation of Gondwana suture zones. *Journal Asian Earth Science* **113**, 826–841.

Takamura Y, Tsunogae T, Santosh M, Malaviarachchi S and Tsutsumi Y (2016) U-Pb geochronology of detrital zircon in metasediments from Sri Lanka: implications for the regional correlation of Gondwana fragments. *Precambrian Research* **281**, 434–452.

Voll G and Kleinschrodt R (1991) Sri Lanka: structural magmatic and metamorphic development of a Gondwana fragment. In *The Crystalline Crust of Sri Lanka. Part I, Summary of Research of the German-Sri Lankan Consortium: Professional Paper no. 5* (eds A Kröner), pp. 22–51. Sri Lanka: Geological Survey Department.

Widanagamage I (2011) EMPA dating of monazite from high grade metamorphic rocks along the Highland-Vijayan boundary zone, Sri Lanka. Kent State University MS thesis, 58 pp.

Williams ML, Jercinovic MJ and Terry MP (1999) Age mapping and dating of monazite on the electron microprobe: deconvoluting multistage tectonic histories. *Geology* **27**, 1023–1026.

Yoshida M, Funaki M and Vitanage PW (1992) Proterozoic to Mesozoic East Gondwana: the Juxtaposition of India, Sri Lanka, and Antarctica. *Tectonics* **11**, 381–391.